JOURNAL OF MATERIALS SCIENCE **38** (2003) 113–118

Crystalline structure and dielectric properties of $(Sr_{1-1.5x}Bi_x)\ TiO_3$ ceramics

ZHI YU*, CHEN ANG*
Department of Materials Science and Engineering, Department of Physics, Zhejiang University, 310027 Hangzhou, People's Republic of China; Department of Ceramics and Glass Engineering, University of Aveiro, 3800 Aveiro, Portugal
E-mail: yxz19@psu.edu

The crystalline structure, microstructure and dielectric properties of the $(Sr_{1-1.5x}Bi_x)TiO_3$ $(0 \leq x \leq 0.267)$ ceramics were studied. Cubic solid solutions were determined for $x \leq 0.2$ at room temperature. However, lattice distortion was detected by Raman spectra. A dense microstructure with the grain sizes of 2–4 μm was obtained for $(Sr_{1-1.5x}Bi_x)TiO_3$ $(0 \leq x \leq 0.2)$ ceramics. The Bi concentration was examined and found to be in agreement with the nominal composition and overall uniformly distributed in the sample. Different from the observations in the earlier literature for other doped quantum paraelectrics, where only an induced dielectric anomaly was reported, there are three Bi induced dielectric modes A, B, and C in the Bi doped $SrTiO_3$ samples. The occurrence of the "impurity modes" and the "ferroelectric relaxor mode" and their evolution are demonstrated as a function of Bi concentration. © *2003 Kluwer Academic Publishers*

1. Introduction

Pure $SrTiO_3$ and $KTaO_3$ display a special dielectric behavior—the so-called quantum paraelectric behavior [1, 2]. No permittivity peaks appear down to 0.03 K. However, permittivity peaks can be induced by introducing substitutional impurities into the lattice [3–6]. For impurity doping studies in quantum paraelectrics, the most common examples are Ca doped $SrTiO_3$ [7] and Li doped $KTaO_3$ [3–6]. But the impurity-induced dielectric permittivity peak was explained controversially by different authors [3–6].

Bi-doped $SrTiO_3$ was first reported in 1950 s by Skanavi *et al*. [8] Smolenskii *et al*. [9] and Gubkin *et al*. [10, 11]. Skanavi *et al*. [8] suggested a polarization mechanism of "hopping ions", rather than occurrence of the ferroelectricity. However, Smolenskii *et al*. [9] and Gubkin *et al*. [10] suggested a ferroelectric mechanism based on the observation of slim electric hysteresis loops.

Recently, the present authors show that Bi-doped $SrTiO_3$ is a good model material to study doping effect in quantum paraelectrics. By a systematic study on the dielectric behavior of Bi-doped $SrTiO_3$, we show an evolution of dielectric behavior from dielectric-relaxor state to ferroelectric-relaxor state with increasing Bi concentration [12–16]. This indicates that the impurity doping effect in quantum paraelectrics is more complicated than supposed before, and Bi doped $SrTiO_3$ is a material in which we can learn more information and clarify some confusions about the doping effect in quantum paraelectrics.

In the previous literature, most studies were limited to the dielectric and ferroelectric-relaxor behavior of $Bi:SrTiO_3$. Detailed information on the crystalline structure and overall dielectric behavior for the Bi doped $SrTiO_3$ system is essential in further understanding the physical mechanism of the system. In this paper we report the crystalline structure by X-ray and Raman studies, the microstructure of Bi doped $SrTiO_3$ ceramics in a wide composition range, and systematically demonstrate the dielectric behavior as a function of Bi concentration.

2. Experimental procedure

In the present work, Sr-site vacancies were introduced in order to maintain the charge equilibrium in Bi doped $SrTiO_3$ sample. The earlier work [8] indicated that trivalent ions Bi^{3+} replaced the divalent Sr^{2+} ions at the A-sites of the perovskite lattice. The nominal composition used in this work is $(Sr_{1-1.5x}Bi_x)\ TiO_3$ with $x = 0$, 0.0005, 0.001, 0.002, 0.0033, 0.0053, 0.0067, 0.0133, 0.0267, 0.04, 0.0533, 0.08, 0.10, 0.133, 0.167, 0.20, 0.227, 0.24 and 0.267, respectively. The ceramic samples were prepared by solid state reaction. The weighed batches were mixed and wet milled. After drying, they were calcined from 1000°C to 1150°C for two hours. The calcined powders were milled again, dried and pressed into disks. Finally, the samples were sintered from 1300°C to 1380°C for two hours in air and furnace-cooled.

The X-ray powder diffraction (XRD) analysis was carried out using an X-ray diffractometer (Rigaku,

Present Address: Materials Research Laboratory, The Pennsylvania State University, University Park, PA16802, USA.

TABLE I The calcining temperature (T_{cal}), sintering temperature (T_s) and dwelling time (t_s) for $(Sr_{1-1.5x}Bi_x)TiO_3$ system. The measured density (D), theoretical density (D_t), and the relative density (D_r) for $(Sr_{1-1.5x}Bi_x)TiO_3$ ceramics

x	T_{cal} (°C)	T_s (°C) × t_s (hrs)	D (g/cm^3)	D_t (g/cm^3)	D_r
0	1150	1400 × 2	5.11	5.12	99.83%
0.0033	1150	1395 × 2	5.08	5.13	99.03%
0.0053	1150	1395 × 2	5.05	5.13	98.44%
0.0067	1150	1390 × 2	5.03	5.13	98.05%
0.0133	1100	1380 × 2	4.78	5.15	92.87%
0.0267	1100	1380 × 2	4.99	5.18	96.41%
0.04	1050	1380 × 2	4.95	5.21	95.03%
0.0533	1050	1350 × 2	4.88	5.23	93.33%
0.08	1000	1350 × 2	4.82	5.29	91.08%
0.10	1000	1300 × 2	5.08	5.33	95.29%
0.133	980	1300 × 2	4.92	5.40	91.15%
0.167	980	1300 × 2	5.00	5.47	91.51%
0.20	950	1300 × 2	5.06	5.53	91.42%
0.227	950	1300 × 2	5.27	–[a]	–[a]
0.24	950	1240 × 2	4.98	–[a]	–[a]
0.267	950	1240 × 2	5.24	–[a]	–[a]

[a]Multiphases.

Geigerflex D/max-C series). The XRD was performed with the scanning speed of 1°/min and the step of 0.02° with the diffraction angle 2θ from 20 to 125 degrees. The microstructures of the polished and thermally etched sections of the samples were observed by using a Hitachi S4100 Scanning Electron Microscope (SEM). Energy Dispersion Spectroscopy (EDS) was performed both at grains and grainboundaries. X-ray line profile analysis was used to detect the distribution of the elements (Sr, Bi and Ti) and any possible segregation at grainboundaries.

3. Synthesis of $(Sr_{1-1.5x}Bi_x)TiO_3$ ceramics

When the mixed powder was calcined and subsequently sintered, the $(Sr_{1-1.5x}Bi_x)TiO_3$ solid solution formed according to the following equations:

$$SrCO_3 + TiO_2 \rightarrow SrTiO_3 + CO_2 \uparrow \quad (1)$$

$$Bi_2O_3 + 3TiO_2 \rightarrow 2Bi^{\bullet}_{Sr} + V''_{Sr} + 3Ti_{Ti} + 9O_O \quad (2)$$

where, the Kröger-Vink notation is adopted. Equation 2 indicates that with the introduction of Bi, the trivalent Bi ions replace divalent Sr^{2+}, forming Sr^{2+}-site vacancies (V_{Sr}) in the solid solution range.

The thermogravimetric (TG) and differential thermal analysis (DTA) were carried out for $(Sr_{1-1.5x}Bi_x)TiO_3$. An endothermic peak occurred around 800–1100°C, which is attributable to the solid state reaction and, correspondingly, the powders lose weight. The maximum relative weight loss is in agreement with the theoretical loss of CO_2, as calculated from Equation 1.

The calcining temperature (T_{cal}), sintering temperature (T_s) and dwelling time (t_s) for the $(Sr_{1-1.5x}Bi_x)TiO_3$ system are shown in Table I. It also shows the measured density (D), theoretical density (D_t) and the relative density (D_r) of the sintered $(Sr_{1-1.5x}Bi_x)TiO_3$ samples, where D was measured by the Archimedes' method and D_t was calculated from the measured lattice parameter as described in the following section 4. It shows that the relative densities of the samples are greater than 90%.

4. Crystalline structure and lattice parameter

4.1. Crystal structure and phases

After sintering, the $(Sr_{1-1.5x}Bi_x)TiO_3$ $(0 \leq x \leq 0.267)$ samples were ground into powders and the phase assemblages were identified by XRD. The typical XRD patterns for the as-sintered samples with $0 \leq x \leq 0.20$ are shown in Fig. 1. The results indicate that the sintered $(Sr_{1-1.5x}Bi_x)TiO_3$ samples with $x \leq 0.20$ are monophasic solid solutions and belong to the cubic crystallographic system. For $x > 0.2$, a small amount of a second phase appeared. The second phase was indentified as $Sr_2Bi_4Ti_5O_{18}$, and the phases $Bi_4(TiO_4)_3$, $Bi_2Ti_4O_{11}$ may also be present (XRD patterns not shown here).

4.2. Lattice parameter

The lattice parameter of the $(Sr_{1-1.5x}Bi_x)TiO_3$ solid solutions with $0 \leq x \leq 0.20$ was calculated using the

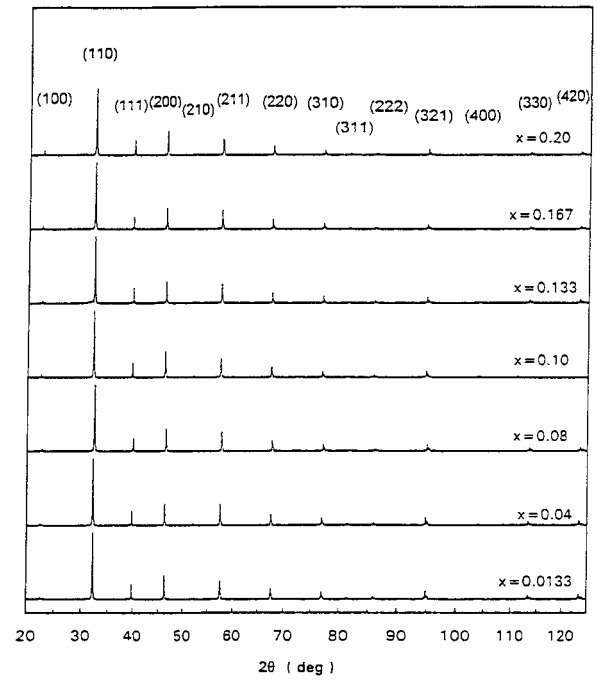

Figure 1 X-ray diffraction patterns for $(Sr_{1-1.5x}Bi_x)TiO_3$ ceramics.

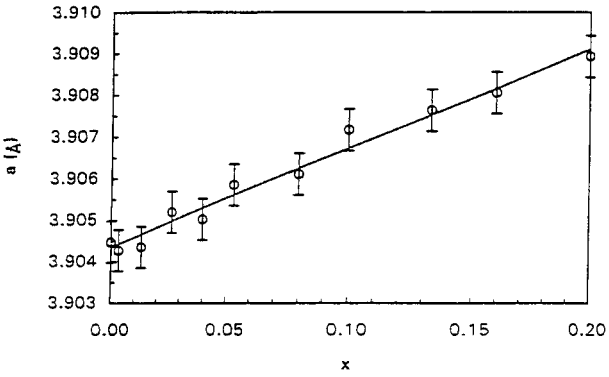

Figure 2 The lattice parameter (a) as a function of x for $(Sr_{1-1.5x}Bi_x)TiO_3$ solid solution.

least square approach, with a standard error less than 5.0×10^{-4}. The lattice parameter as a function of Bi content is shown in Fig. 2. The lattice parameter of $(Sr_{1-1.5x}Bi_x)TiO_3$ solid solutions increases with increasing Bi concentration.

4.3. Raman spectra

Although the XRD results showed that the doped samples have a cubic structure at room temperature, similar to that of pure $SrTiO_3$, the dielectric behavior indicated that there are some induced dielectric peaks (see below). This implies that the lattice distortion may be induced by Bi doping. The typical Raman spectra for the $(Sr_{1-1.5x}Bi_x)TiO_3$ samples with $x = 0.0133, 0.04, 0.10$, and 0.167 at 50 K and 300 K are shown in Fig. 3a and b, respectively. It can be seen that at the room temperature, some non-activated modes for pure $SrTiO_3$ become activated for the Bi doped $SrTiO_3$ (as indicated by arrows), although all the samples have a cubic symmetry at room temperature by the XRD results. The intensities of these first-order lines increase with increasing Bi concentration, implying that the lattice distrotion from cubic to tetragonal symmetry was strengthened.

5. Microstructure

5.1. Microscopic morphology and grain size

The microphotographs of the polished and thermally-etched sections of $(Sr_{1-1.5x}Bi_x)TiO_3$ solid solutions with $x = 0.0133$, 0.0267, 0.0533 and 0.10 are shown in Fig. 4a–d, respectively. The calculated average grain sizes are ~2–4 μm for all the solid solutions and no systematic variation of the grain size was observed with increasing Bi concentration.

5.2. Examination of the Bi concentration

SEM/EDS analysis was carried out on the polished and thermally etched sections and on the fractures of the solid solutions in order to determine the Bi, Ti, and Sr concentration. More than five areas were examined and the average atomic percentage of each element was calculated. The data are illustrated in Table II. The results show that the Bi concentration detected by EDS in different areas including grains and grain-boundaries is uniform and close to the nominal concentration is small, i.e., less than 5%, which is acceptable.

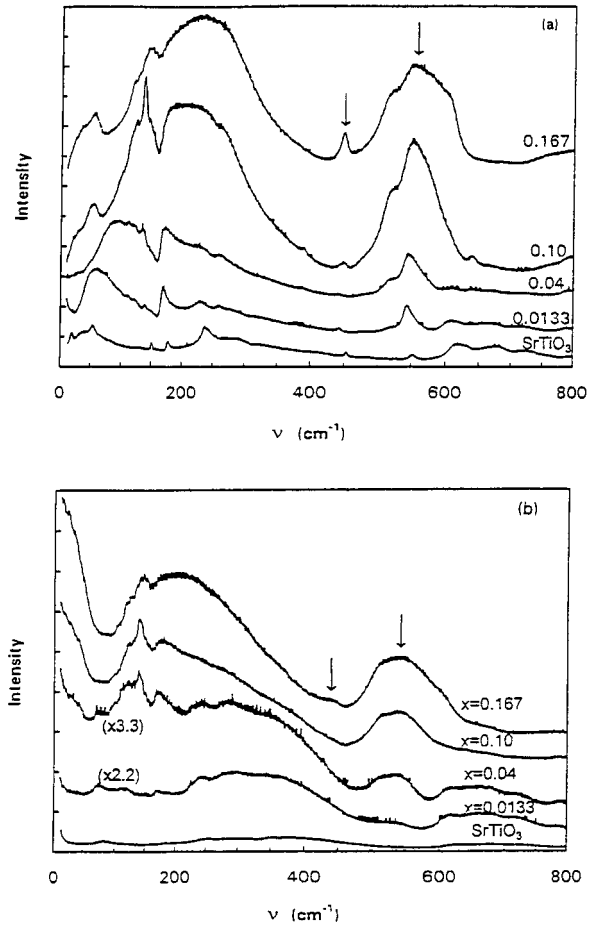

Figure 3 Raman spectra of $(Sr_{1-1.5x}Bi_x)TiO_3$ ceramics with $x = 0$, 0.0133, 0.04, 0.1, and 0.167 at 50 K (a) and 300 K (b). The labels in brackets are the magnification scale.

5.3. Distribution of elements

The X-ray line profile analysis crossing over several grains and grain-boundaries was performed on SEM for the solid solutions. The typical X-ray line profiles for the elements Sr, Bi and Ti in the sample with $x = 0.0533$ are shown in Fig. 5. It can be seen that the distribution of Sr, Bi and Ti is uniform and no obvious segregation of any elements, either on the grain or grain boundaries, was detected.

In a word, the SEM, EDS and X-ray line profile analyses for the as-sintered samples of the $(Sr_{1-1.5x}Bi_x)TiO_3$ solid solutions show that either segregation or loss of Bi is small, i.e., less than 5% of dopant concentration.

6. Dielectric properties and discussion

The temperature dependence of the dielectric constant at 100 Hz for all the $(Sr_{1-1.5x}Bi_x)TiO_3$ solid solutions is shown in Fig. 6. Fig. 7 shows plots of ε vs T at different frequencies for some typical compositions with $x = 0.002$, 0.0133 and 0.08 (see below). It can be seen that for different Bi doping concentration, the samples exhibit different dielectric behavior. In nominally pure $SrTiO_3$ ceramics, the dielectric permittivity continuously increases with decreasing temperature until ~12 K, and then levels off to the lowest temperature 1.5 K used in this work. However, in Bi doped ST, the dielectric responses show that there are three Bi induced dielectric modes A, B, and C in the samples.

TABLE II The atomic percentage (P) of Ti, Sr and Bi atoms for $(Sr_{1-1.5x}Bi_x)TiO_3$ samples detected by EDS (P_{exp}, the experimental value detected; P_{nom}, the nominal compositional value)

x		Bi	Ti	Sr
0.0133	P_{exp}	0.64 at.%	56.55 at.%	42.82 at.%
	P_{nom}	0.67 at.%	50.17 at.%	49.16 at.%
	$(P_{nom} - P_{exp})/P_{nom}$	4.5%	−12.7%	12.9%
0.0267	P_{exp}	1.32 at.%	57.17 at.%	41.51 at.%
	P_{nom}	1.34 at.%	50.34 at.%	48.32at.%
	$(P_{nom} - P_{exp})/P_{nom}$	1.5%	−13.6%	14.1%
0.0533	P_{exp}	2.70 at.%	53.89 at.%	43.42 at.%
	P_{nom}	2.70 at.%	50.68 at.%	46.62 at.%
	$(P_{nom} - P_{exp})/P_{nom}$	0%	−6.3%	6.9%
0.133	P_{exp}	6.62 at.%	54.01 at.%	39.37 at.%
	P_{nom}	6.90 at.%	51.72 at.%	41.38 at.%
	$(P_{nom} - P_{exp})/P_{nom}$	4.0%	−4.4%	4.9%

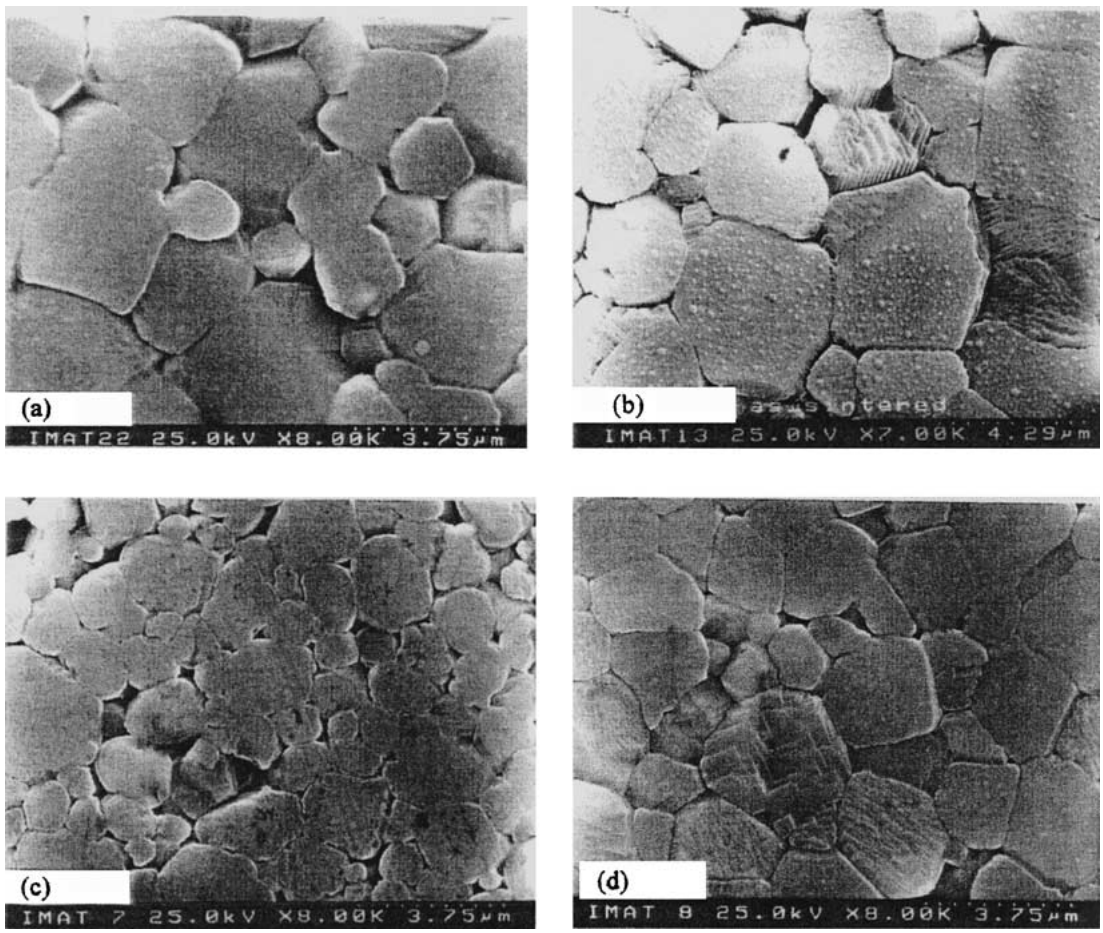

Figure 4 Microphotographs of the polished and thermally-etched sections of $(Sr_{1-1.5x}Bi_x)TiO_3$ ceramics with $x = 0.0133$ (a), 0.0267 (b), 0.0533 (c), 0.10 (d).

1. *Low level Bi doped samples ($0.0005 \leq x \leq 0.002$).* Two dielectric anomalies at ∼18 K and ∼30 K (at 100 Hz), denoted as modes A and B, are induced. The two dielectric anomalies are frequency dependent. However, it should be emphasized that their T_m are independent of Bi concentration, and the relaxation times follow the Arrhenius law [14]. These peaks were named as "impurity modes" (or "defect modes"), which are superimposed upon the quantum paraelectric background of ST [13, 14, 16].

2. *Middle level Bi doped samples ($0.0033 \leq x \leq 0.0133$).* As Bi concentration exceeds 0.002, mode C appears. The amplitude of this peak increases monotonically with increasing Bi concentration. It should be emphasized that the T_m of mode C increases with increasing Bi concentration, which is different from those of modes A and B. The relaxation time of mode C follows the Vogel–Fulcher law, hence the mode C is attributed to "ferroelectric relaxor mode" [15]. In the range of $0.0033 \leq x \leq 0.0133$, the coexistence of the "defect modes" and "ferroelectric relaxor mode" is a characteristic of the $(Sr_{1-1.5x}Bi_x)TiO_3$ solid solutions.

3. *High level Bi doped samples.* When Bi concentration further increases, as $x \geq 0.04$, mode C dominates. Mode A at ∼18 K disappears at $x > 0.0133$. Mode B at ∼30 K becomes very small at $x = 0.04$ and disappears

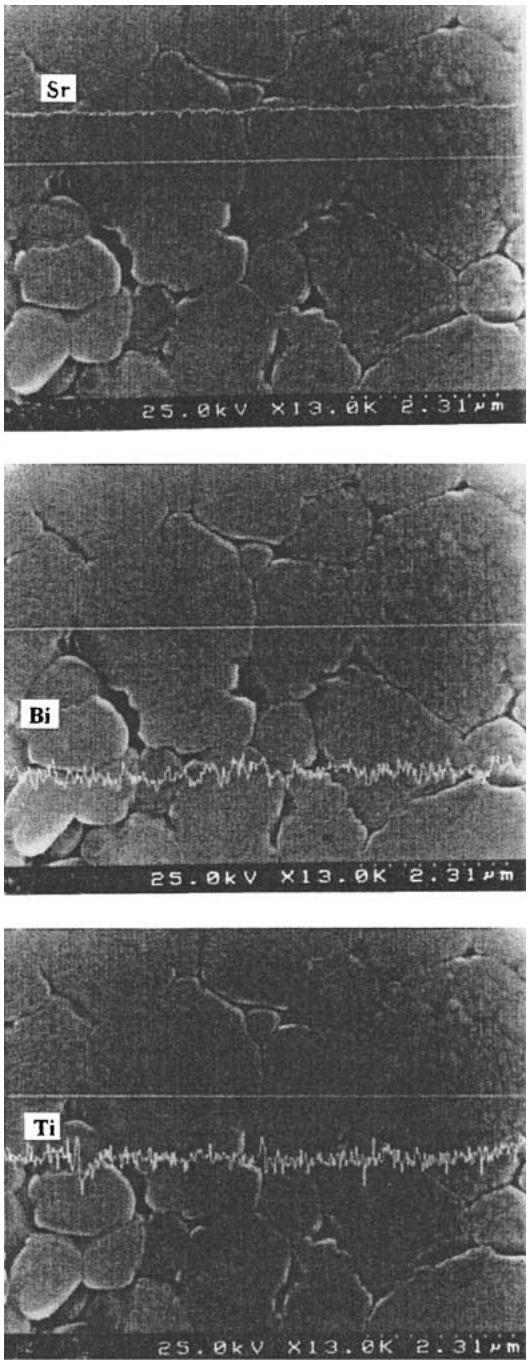

Figure 5 SEM X-ray line profiles of the elements Sr, Bi, and Ti for $(Sr_{1-1.5x}Bi_x)TiO_3$ ceramics with $x = 0.0533$.

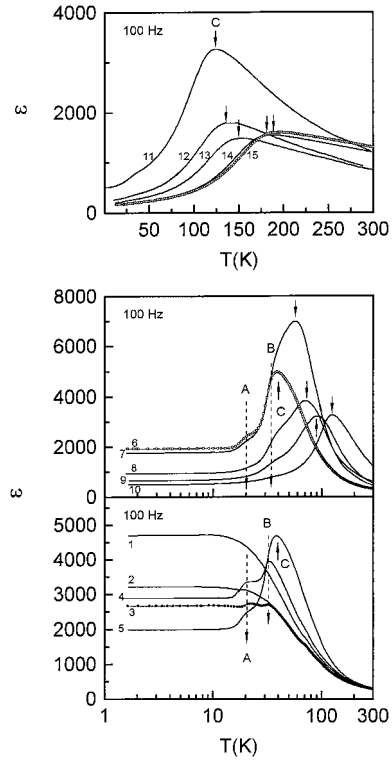

Figure 6 The temperature dependence of the dielectric constant at 100 Hz for the all $(Sr_{1-1.5x}Bi_x)TiO_3$ samples. 1: $x = 0$, 2: $x = 0.0005$, 3: $x = 0.001$, 4: $x = 0.002$, 5: $x = 0.0033$, 6: $x = 0.0053$, 7: $x = 0.0067$, 8: $x = 0.0133$, 9: $x = 0.0267$, 10: $x = 0.04$, 11: $x = 0.0533$, 12: $x = 0.08$, 13: $x = 0.1$, 14: $x = 0.167$, 15: $x = 0.2$.

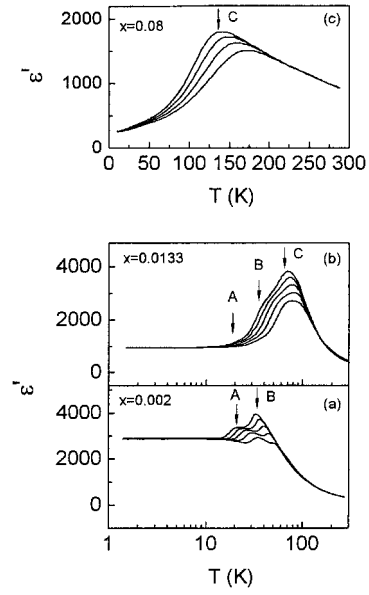

Figure 7 The temperature dependence of the dielectric constant at different frequencies (from top to bottom, 100 Hz, 1 kHz, 10 kHz, 100 kHz, and 1 MHz) for the samples with $x = 0.002$, 0.0133 and 0.08.

at $x \geq 0.133$. For $x \geq 0.133$, the system shows a typical "ferroelectric relaxor" behavior, which can be clearly seen in Fig. 7c.

The above observed results indicate complicated dielectric behavior in Bi doped quantum paraelectric $SrTiO_3$. The samples with different Bi concentration have different polarization mechanisms, which can not be simply attributed to a "hopping ions" polarization suggested by Skanavi *et al*. [8] or a "ferroelectric relaxor" polarization mechanism proposed by Smolenskii *et al*. [9].

On the other hand, impurity induced dielectric anomaly in doped quantum paraelectrics, for example, $Li : KTaO_3$ and $Ca : SrTiO_3$, has been extensively studied in the literature [3–6], and generally only one induced dielectric peak was reported and discussed. However, people found that the theoretical critical concentration of impurity for the occurrence of the long range order is far lower than the experimental value [17]. In the present work, multi-polarization mechanisms were induced by Bi doping in the quantum paraelectric $SrTiO_3$. This implies that a revisit for the dielectric behavior of $Li : KTaO_3$ and $Ca : SrTiO_3$ would be interesting.

In addition, Bi doped $SrTiO_3$ also gives a composition-controlled example for the occurrence of the "impurity mode" and the "ferroelectric relaxor mode" and their evolution with variation of Bi concentration. The Bi doped $SrTiO_3$ system might be a good model material to study the doping effect of the quantum paraelectrics and the physical mechanism of ferroelectric relaxors.

7. Conclusions

The $(Sr_{1-1.5x}Bi_x)TiO_3$ $(0 \leq x \leq 0.267)$ ceramics were synthesized and their microstructure and crystal structure were studied. The limit of solid solubility of Bi ions is identified as $x = 0.2$. The XRD results show that the samples with $x \leq 0.2$ belong to cubic symmetry at room temperature, and the lattice parameter increases with increasing Bi concentration as $x \leq 0.20$. Raman spectra indicate that the lattice distortion from cubic toward tetragonal symmetry was strengthened with increasing Bi concentration. The SEM, EDS and X-ray line profiles show that, for all solid solution samples, the Bi concentration is in agreement with the nominal composition, and the distribution of Sr, Bi, and Ti ions is overall uniform. The grain size ranged from 2 to 4 μm without obvious dependence on the Bi concentration for $(Sr_{1-1.5x}Bi_x)TiO_3$ $(0 \leq x \leq 0.2)$ ceramics.

Different from the observations in the earlier literature for other doped quantum paraelectrics, where only an induced dielectric anomaly is reported, the occurrence of the Bi induced "impurity modes" and the "ferroelectric relaxor mode" and their evolution with variation of Bi concentration are observed as a function of Bi concentration.

Acknowledgments

The author would like to thank Prof. J. L. Baptista for the stimulating discussion, and thank Dr. Li-jian Meng for his help in the measurement of Raman spectra. The sample preparation performed mainly in Zhejiang University was supported by the Science and Technology Committee of Zhejiang Province, P. R. China and the characterization of the samples mainly carried out in the University of Aveiro was supported by the Praxis XXI, JNICT, Portugal.

References

1. M. E. LINES and A. M. GLASS, "Principles and Applications of Ferroelectrics and Related Materials" (Oxford University Press, 1977) ch. 8.
2. K. A. MÜLLER and H. BURKHARD, *Phys. Rev.* B **19** (1979) 3593.
3. G. A. SAMARA, *Phys. Rev. Lett.* **53** (1984) 298.
4. Y. YACOBY, *Z. Phys.* B **41** (1981) 269.
5. J. TOULOUSE, P. DIANTONIO, B. E. VUGMEISTER, X. M. WANG and L. A. KNAUSS, *Phys. Rev. Lett.* **68** (1992) 232.
6. W. KLEEMANN, S. KÜTZ and D. RYTZ, *Europhys. Lett.* **4** (1987) 239.
7. J. G. BEDNORZ and K. A. MÜLLER, *Phys. Rev. Lett.* **52** (1984) 2289.
8. G. I. SKANAVI and E. N. MATVEEVA, *Sov. Phys. JETP* **3** (1957) 905; G.I. SKANAVI, I. M. KSENDZOV, V. A. TRIGUBENKO and V. G. PROKHVATILOV, *ibid.* **6** (1958) 250.
9. G. A. SMOLENSKII, V. A. ISUPOV, A. I. AGRANOVSKAYA and S. N. POPOV, *Sov. Phys.: Solid State* **2** (1967) 2584.
10. A. N. GUBKIN, A. M. KASHTANOVA and G. I. SKANAVI, *ibid.* **3** (1961) 807.
11. A. N. GOBKIN, *ibid.* **2** (1961) 2732.
12. CHEN ANG, ZHI YU, P.M. VILARINHO and J. L. BAPTISTA, *Phys. Rev.* B **57** (1998) 7403.
13. CHEN ANG, J. F. SCOTT, ZHI YU, H. LEDBETTER and J. L. BAPTISTA, *ibid.* **59** (1999) 6661.
14. CHEN ANG, ZHI YU, J. HEMBERGER, P. LUNKHEMER and A. LOIDL, *ibid.* **59** (1999) 6665.
15. CHEN ANG, ZHI YU, P. LUNKHEMER, J. HEMBERGER and A. LOIDL, *ibid.* **59** (1999) 6670.
16. CHEN ANG and ZHI YU, *J. Appl. Phys.* **91** (2002) 1487.
17. B. E. VUGMEISTER and M. D. GLINCHUK, *Rev. Mod. Phys.* **62** (1990) 993; B. E. VUGMEISTER and M. D. GLINCHUK, *Sov. Phys. JETP* **52** (1980) 3.

Received 16 July 2001
and accepted 6 May 2002